KTH Electrical Engineering

MEMS tunable polarization rotator for optical communication

Sandipan Das

Stockholm, March 1, 2016

Contents

1 Introduction **1**
1.1 Optical communication . . . 1
1.2 Silicon photonics . . . 2
1.3 Motivation . . . 4
1.4 Objectives . . . 5
1.5 Outline of this thesis . . . 5

2 State of the art **6**
2.1 Optical waveguide theory . . . 6
2.1.1 Maxwell's equations . . . 6
2.1.2 Optical waveguides . . . 9
2.1.2.1 Planar waveguides . . . 9
2.1.2.2 Channel waveguides . . . 10
2.1.3 Snell's law and total internal reflection . . . 11
2.1.4 Eigenvalue and wave modes . . . 12
2.1.5 Optical polarization and transverse modes . . . 13
2.1.5.1 TE mode . . . 14
2.1.5.2 TM mode . . . 14
2.1.6 Confinement factor . . . 15
2.1.7 Jones calculus . . . 16
2.1.7.1 Jones vector . . . 16
2.1.7.2 Jones matrix . . . 17
2.1.8 Jones matrix for polarizing optical systems . . . 17
2.1.8.1 Polarizer . . . 17
2.1.8.2 Wave plates . . . 18
2.1.9 Poincaré sphere and state of polarization . . . 18
2.1.10 Stoke's parameter . . . 19
2.1.11 Coupling mode theory . . . 21
2.2 Polarization tuning in optical waveguide . . . 23
2.2.1 Thermo-optic mechanism . . . 23
2.2.2 Electro-optic mechanism . . . 23
2.2.3 Liquid crystals . . . 23
2.2.4 Current injection . . . 23
2.2.5 MEMS . . . 23
2.3 Polarization rotator (PR) . . . 23
2.3.1 Optical fiber PR . . . 23

2.3.2 On-chip PR . . . 23
2.3.2.1 Passive PR . . . 23
2.3.2.2 Active PR . . . 28

3 Design and simulation **31**
3.1 Approach . . . 31
3.2 Designing the experiment . . . 31
3.2.1 Design principle . . . 31
3.2.2 Design A: . . . 31
3.2.3 Design B: . . . 31
3.2.4 Design C: . . . 31
3.3 Choice of simulation . . . 31
3.4 Simulation results and analysis . . . 31

4 Fabrication **32**

5 Interpreting the results **33**
5.1 Experimental setup for measurement . . . 33
5.2 Results . . . 33
5.3 Analysis . . . 33

6 Discussion **34**
6.1 Limitations . . . 34
6.2 Future work . . . 34

7 Conclusions **35**

Abbreviations **37**

Bibliography **39**

Chapter 1
Introduction

1.1 Optical communication

Communication and collective thinking are the key to the development of human civilization. This development is driven by data - "The new oil of this digital era". With the advent of Internet of Things (IoT), there has been a huge surge in data traffic all over the world. It has been estimated that by 2020 there will be 26 billion connected devices [1], and all devices that can be connected will be connected. Ericsson's mobility report [2] estimates that 70% of world's population will use smart-phones by 2020 and 90% of the world's population over 6 years old will have a mobile phone by 2020. Today, only about 40% [3] of the world's population use the internet. With time, data traffic is poised to grow exponentially as shown in Fig. 1.1, as per Ericsson [4].

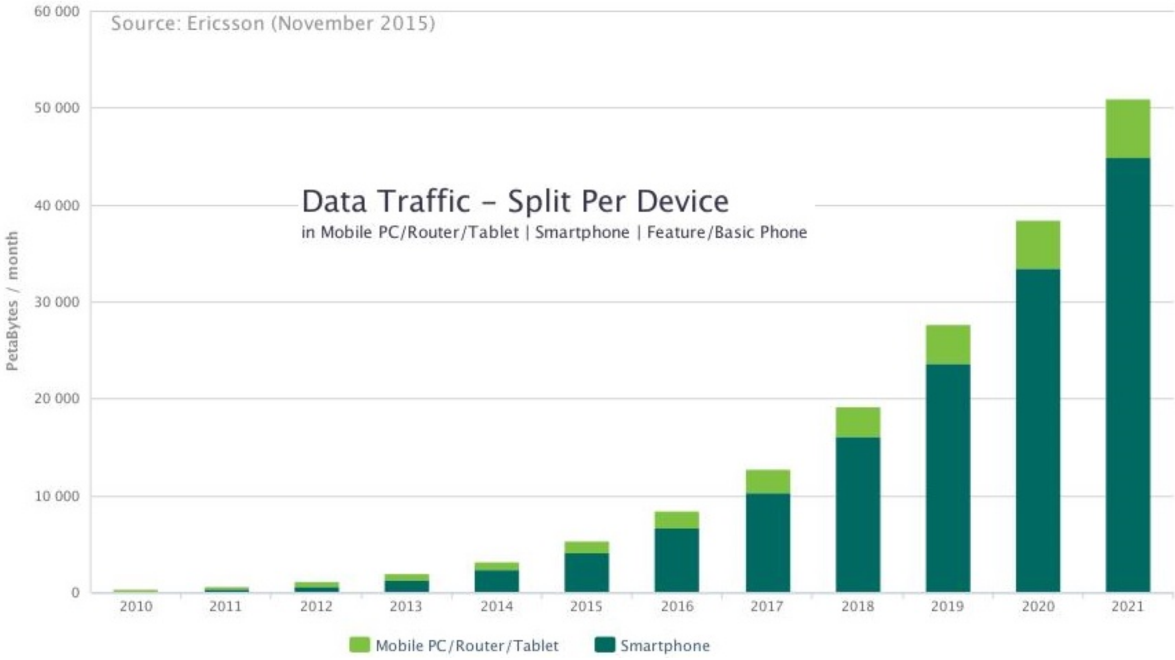

Figure 1.1: Data traffic growth forecast by 2020, as per Ericsson, generated using [4, 5]

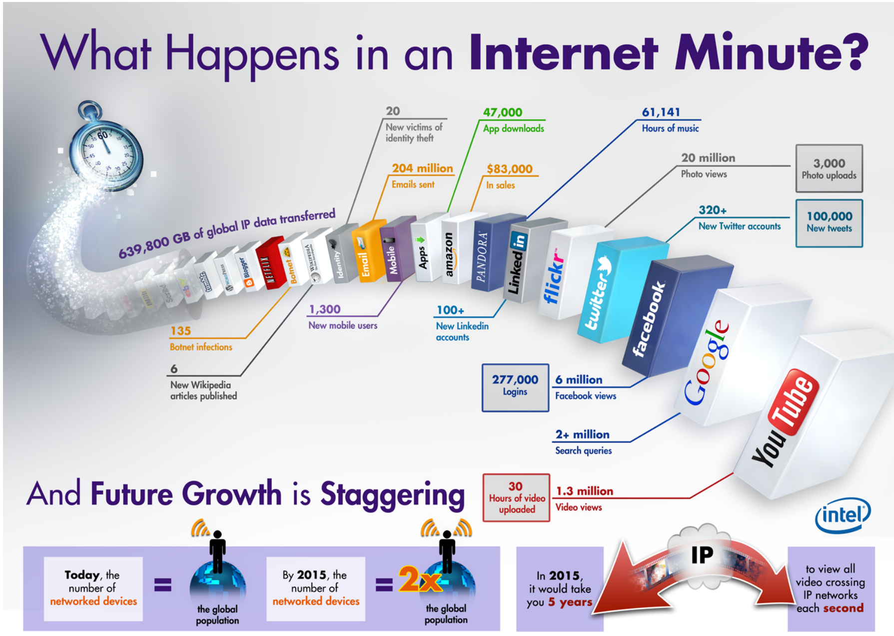

Figure 1.2: What happens on internet per minute [5]

As illustrated in Fig. 1.2, it is evident that huge data is processed per minute due to different Information and communication technology (ICT) services. Eventually, as more and more people use the different ICT services this data growth will be higher than ever. In consequence, the telecommunications industry is moving towards IP Multimedia Subsystem (IMS) core networks which is a transition towards full IP based networks. So how is this traffic managed? The answer is the optical fiber, which serves as the backbone of all the communication systems. Optical fiber is chosen over previously used copper cables for the following reasons:

- ☐ Fiber provides more bandwidth than copper and has standardized performance up to 100 Gbps and beyond, with very low power consumption.
- ☐ Fiber is less susceptible to temperature fluctuations than copper and can be submerged in water for intercontinental long distance communication. Unlike copper, it's immune to Electromagnetic (EM) interference.
- ☐ It doesn't radiate signals and is extremely difficult to tap, which provides better security than copper cables.
- ☐ Fiber optic transmission results in less attenuation (losses) than copper cables.

Less than copper...verify

1.2 Silicon photonics

The performance of optical fiber networks is remarkable and it is this backbone which gives us a great user experience. The current internet architecture has already pushed the optical fiber to the network edges and the trend is to push it as closer to the processor as possible. This has already opened up a new trend of "siliconizing photonics" [6], which arose from the decades of research from microelectronics industry.

The electronics industry has pushed the boundaries of the processing speed of Integrated circuit(s) (IC) according to Moore's Law. Until recently, exponential increases in the speed, efficiency, and processing power of conventional electronic devices were achieved largely through the downscaling and clustering of components on a chip. However, this trend toward miniaturization has yielded unwanted effects in the form of significant increases in noise, power consumption, signal propagation delay and aggravates already to serious thermal management problems. Alternatively, the wires can be made thicker, but then the packing density will be inefficient. As a result, traditional microelectronics will soon fall short of meeting market needs, inhibited by the thermal and bandwidth bottlenecks inherent in copper wiring. Intel processor speed and bus speed comparison shows that although we have achieved good processing speed, the interconnects always find difficulty in catching up with the processing speed [7]. Annual global data center IP traffic will reach 10.4 zettabytes (863 exabytes per month) by the end of 2019, up from 3.4 zettabytes per year (287 exabytes per month) in 2014 [8]. Think of a server rack in a data center processing an average of this huge data per second, where interconnects between processors in the server rack add up to a significant bottleneck. These bottlenecks can be overcome by substituting copper with optical interconnects using the current technology, which can also operate at low power and better efficiency. In addition optical interconnects can also reduce heat dissipation, switching and transmission of electrical signals.

Although silicon is the material of choice for electronics, only from late 1980s silicon is being considered as a practical option for Optoelectronic integrated circuit (OEIC) solutions. Silicon has many properties that make it a good material for optics. First of all, the band gap of silicon ($\sim$1.1 eV) is such that the material is transparent to wavelengths commonly used for optical communication ($\sim$1.3 µm-1.6 µm). Moreover, one can use standard Complementary metal-oxide semiconductor (CMOS) processing techniques to sculpt optical waveguides onto the silicon surface. Similar to an optical fiber, these waveguides can be used to confine and direct light as it passes through the silicon [9] using total internal reflection. Due to the wavelengths typically used for optical transport and silicon's high index of refraction, the feature sizes needed for processing these silicon waveguides are on the order of 0.5 µm-1 µm. This makes silicon excellent for miniaturization of optical components. The fabrication and lithography requirements needed to process waveguides with these sizes exist today. Finally, it is CMOS-compatible, making it possible to process monolithic optical devices, which could bring new levels of performance, functionality, power and size reduction, all at a lower cost.

Today silicon photonics is a new approach to make miniaturized optical devices that use light to move huge amounts of data at very high speeds with extremely low power over a thin optical fiber rather than using electrical signals over a copper wire. Since already a large capital investment has been done on perfecting the current fabrication technology and infrastructure, engineers are working on creating monolithic design of integrated circuits which will use light instead of electric signals [10]. Research institutes and industry, are trying to bridge this gap by creating highly integrated photonic and electronic components that combine the functionality of conventional CMOS circuits with the significantly enhanced performance of photonic solutions. Various kinds of silicon photonic devices, such as switches [11, 12, 13, 14], modulators [15, 16], photo-detectors [17, 18], delay lines [19, 20], sensors [21, 22, 23] etc. have been reported till date. This leads to a booming silicon photonics market, which is estimated to grow to 700 million USD by 2024 [24, 25] with a Compound annual growth rate (CAGR) of 38%.

1.3 Motivation

To keep up with bandwidth requirements using existing network infrastructure, spatial-division multiplexing technique [26] is being contemplated, which uses multimode transmission. However, simply connecting the end of such fibers to an OEIC is far more complicated than standard fibers, because much more mechanical precision is required. Great care has to be taken to make sure light goes in exactly as intended [27]. Moreover, all photonic devices based on silicon waveguides are sensitive to polarization due to large structural birefringence, which induces substantial Polarization dependent loss (PDL), Polarization mode dispersion (PMD), and other Polarization dependent wavelength characteristics (PDλ), limiting their usability. Also, in a complex OEIC system, polarization is a major issue because power can be exchanged between the polarization states in the presence of junctions, tapers, slanted sidewalls, bends, or other discontinuities. Therefore, sometimes, it is necessary to have a fixed degree of polarization state, and it may also be necessary to rotate an incoming polarization state.

To overcome these challenges, Polarization rotator (PR) is engineered on silicon for OEIC and various designs have already been demonstrated [28, 29, 30, 31, 32, 33, 34]. The main working principle of these proposed solutions is introducing asymmetry in the waveguide structure. However, in some cases, the designs [35], if used in commercial applications for miniature interconnects, would incur inefficient packing density since too much space is required to achieve high and robust tuning. Apart from that there might also be thermo-optic cross-talk problem which might change phase of the wave in other waveguides in high compact density environment as silicon is highly susceptible to thermal changes [36]. Also, a Tunable polarization rotator (TPR) has been reported which works on the principle of Berry's phase, a quantum-mechanical phenomenon of purely topological origin [37]. For PR, the design uses out-of-plane ring cavity which inherits the narrow band spectral features of ring resonator limiting the bandwidth. Phase tuning is achieved through thermo-optic effect which has its limitations. The general goal of the thesis work is to realize an efficient TPR using Microelectromechanical systems (MEMS) in C and L bands, at low power, with high precision and accuracy.

1.4 Objectives

Main objective: To design and fabricate low power TPR based on MEMS tuning.

Sub objectives: The areas which will be addressed are:

- ☐ Feasibility of the idea and the strategy to design the TPR.
- ☐ Design and simulation of the device.
- ☐ Fabrication and characterization of the MEMS TPR.

1.5 Outline of this thesis

The outline of the thesis is as follows: Background, motivation and the research questions being addressed, is discussed in Chapter 1. In Chapter 2, the current state of art for the available solution is discussed along with the background literature required. Here, also the working principle of the current available design are explained along with the areas which can be improved. Chapter 3 discusses about the design of the final system and the results obtained about the simulation setup. In Chapter 4, documentation about the fabricated design is provided along with currently available standard fabrication technologies. Results and characterization are an important part of the work, which is discussed in Chapter 5. Finally, Chapter 6 and 7 discusses about the future work possibilities respectively along with the known limitations and conclusion of the system if any.

Chapter 2

2 State of the art

To understand the working principles of PR it is important to look into the basic concepts of waveguides and the mathematics behind the propagation of EM waves. It is also necessary to understand tuning of optical waveguides using different mechanisms to achieve optical PR. Finally, the integrated PRs found in the recent literature and their underlying concepts are discussed.

2.1 Optical waveguide theory

Light can travel through dielectric waveguide. To comprehend the situation we need to look at the physical properties of light and waveguides. The basic understanding of Maxwell's equations is required. Maxwell combined the electric and magnetic fields in a wave equation. Since we need a formal definition of the different State of polarization (SOP), described using Jones calculus. Moreover, the rotation from one SOP to another, can be defined formally on the Poincaré sphere.

2.1.1 Maxwell's equations

Wave is a disturbance that propagates through a medium. Waves transfer both energy and momentum, without transferring any mass. EM radiation is the radiant energy released by varying EM field. Light wave is EM radiation at very high frequency. The frequency of visible light falls in between IR and UV EM wave. James Clerk Maxwell discovered that he could combine four simple equations, which had been previously discovered, along with a slight modification to describe self-propagating waves of oscillating electric and magnetic fields [38]. The understanding of propagating of light waves using Maxwell's equations in a dielectric medium, is the key to the construction of waveguides. Maxwell's equations relate the electric field E (V/m), magnetic field H (A/m), charge density ρ (C/m3), and current density J (A/cm2).

- **Maxwell's first equation (Gauss' Law)**: The net electric flux through any closed surface is equal to $\frac{1}{\epsilon_m}$ times the charge density within that closed surface.

$$\nabla . E = \frac{\rho}{\epsilon_m} \tag{2.1}$$

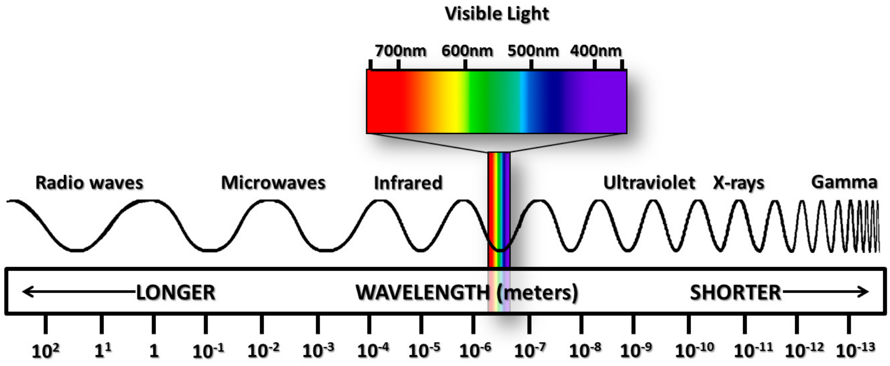

Figure 2.1: The EM wave spectrum

where ϵ_m the permittivity of the medium, and del operator, ∇, is given by:

$$\nabla = \left(\frac{\partial i}{\partial x}, \frac{\partial j}{\partial y}, \frac{\partial k}{\partial z} \right) \tag{2.2}$$

where i, j and k are unit vectors in the x, y and z directions respectively.

- **Maxwell's second equation (Gauss' Law for magnetic field)**: The net magnetic flux through a closed surface is always zero since magnetic monopoles do not exist.

$$\nabla . H = 0 \tag{2.3}$$

- **Maxwell's third equation (Faraday's law)**: Induced electric field around a closed path is equal to the negative of the time rate of change of magnetic flux enclosed by the path.

$$\nabla \times E = -\mu_m \frac{\partial H}{\partial t} \tag{2.4}$$

where μ_m is the magnetic permeability of the medium.

- **Maxwell's fourth equation (Modification of Ampere's law)**: The fourth equation states that magnetic fields can be generated in two ways: by electric current (this was the original "Ampere's law") and by changing electric fields (this was "Maxwell's addition") [39].

$$\nabla \times H = J + \epsilon_m \frac{\partial E}{\partial t} \tag{2.5}$$

where ϵ_m is the electric permittivity of the medium.

These equations combine into the following wave equation

$$\nabla^2 E - \mu_m \epsilon_m \frac{\partial^2 E}{\partial t^2} = \mu_m \frac{\partial J}{\partial t} + \frac{\nabla \rho}{\epsilon_m}, \tag{2.6}$$

using the curl of curl identity operation given by

$$\nabla^2 E = \nabla(\nabla.E) - \nabla \times (\nabla \times E). \tag{2.7}$$

A general solution to the equation 2.6 in free space, in absence of charge is

$$\overrightarrow{E}(z,t) = E_0(x,y)e^{i(\omega t \pm k_0 z)}, \tag{2.8}$$

where z is direction of propagation of wave in Cartesian coordinates, phase, $\phi = \omega t \pm k_0 z$ and wave vector propagation constant, $k_0 = \dfrac{\partial \phi}{\partial t} = \dfrac{2\pi}{\lambda}$, in the direction of propagation of the wave. The propagation constant in medium varies according to n_{eff}, the effective Refractive index (RI) of the medium and is given by

$$k = n_{eff} k_0, \tag{2.9}$$

where

$$n_{eff} = \sqrt{\varepsilon_m \mu_m}. \tag{2.10}$$

Similar calculations for the magnetic field, H in free space yields,

$$\overrightarrow{H}(z,t) = H_0(x,y)e^{i(\omega t \pm k_0 z)} \tag{2.11}$$

In the Fig. 2.2 the electric field and magnetic field propagate in directions perpendicular to each other. Moreover, the direction of propagation is also transverse to the EM field. Hence it is called Tansverse Electromagnetic (TEM) wave.

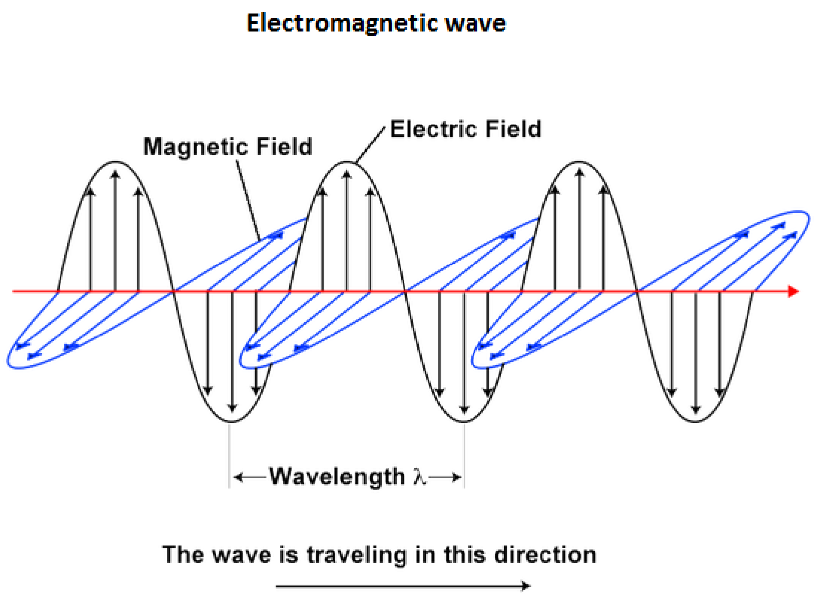

Figure 2.2: Propagation of EM wave

2.1.2 Optical waveguides

The waveguide is the essential element of every photonic circuit which can be characterized by the number of dimensions in which light is confined inside it [40]. A planar waveguide confines light in 1-D, which is simple for understanding of the wave propagation using Maxwell's equations. However, for practical applications 2-D confinement is necessary and that is why channel waveguides are used. Structures like photonic crystals even have 3-D confinement properties.

2.1.2.1 Planar waveguides

A simple planar waveguide consists of a high-index medium with height h surrounded by lower-index materials on the top and bottom sides, known as cladding. The RI of the film is n_f. The RI of the substrate in lower cladding is n_s whereas, RI of the substrate in upper cladding is n_c.

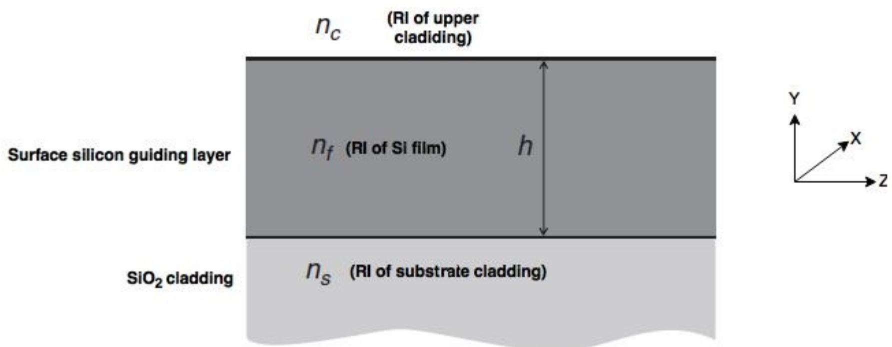

Figure 2.3: A typical planar waveguide where the film is infinite in XZ-plane

For planar waveguides the wave equation for electric field (2.8) and magnetic field (2.11) can be rewritten as follows:

$$\begin{cases} \overrightarrow{E}(z,t) = E_x(y)e^{i(\omega t \pm k_0 z)} \\ \overrightarrow{H}(z,t) = H_x(y)e^{i(\omega t \pm k_0 z)} \end{cases} \tag{2.12}$$

since in X-direction the film is infinite. After using the homogeneous wave equations for a planar waveguide the following Transverse Electric (TE) and Transverse Magnetic (TM) mode equations can be deduced:

$$\begin{cases} \nabla^2 E_x(y) + (k_0^2 n(y)^2 - k^2)E_x(y) = 0 \\ \nabla^2 H_x(y) + (k_0^2 n(y)^2 - k^2)H_x(y) = 0 \end{cases} \tag{2.13}$$

where $n(y)$ depends only on a single Cartesian coordinate $n_{eff} = n(y)$. These equations can be solved analytically using the various boundary conditions of the waveguides which help in deducing the nature of propagation of the wave in TE and TM mode.

Different kinds of numerical methods like Finite element method (FEM), Finite integration technique (FIT), Finite difference time domain (FDTD), Beam propagation method (BPM) have been developed to decipher the nature of light propagation in waveguides.

2.1.2.2 Channel waveguides

As mentioned earlier channel waveguides provide confinement in 2-D which helps in analyzing waveguides in a more practical way. The three main types of channel waveguides are rib, strip and buried waveguides. As depicted in 2.4a, 2.4b, 2.4c the different conceptual structures of the waveguides can be envisaged. While the rib and strip waveguides are designed using etching techniques, the buried waveguide mostly relies on diffusion and epitaxial growth techniques for its fabrication.

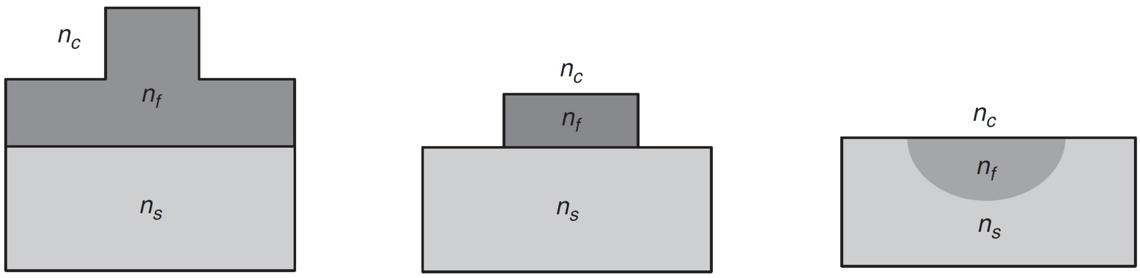

(a) Rib waveguide (b) Strip waveguide (c) Buried waveguide

Figure 2.4: Different kinds of design for channel waveguides

- **Design rules of rib waveguides:** While designing these waveguides each of these have specific design rules for optimum performance and low-loss coupling, which has been standardized after years of research [40]. The Single-mode condition (SMC) for *rib waveguides* is as follows:

$$\frac{W}{H} \leq 0.3 + \frac{r}{\sqrt{1-r^2}}, \quad \text{for } (0.5 \leq r < 1) \tag{2.14}$$

where W=waveguide width, H=rib height, r is ratio of slab height to overall rib height.

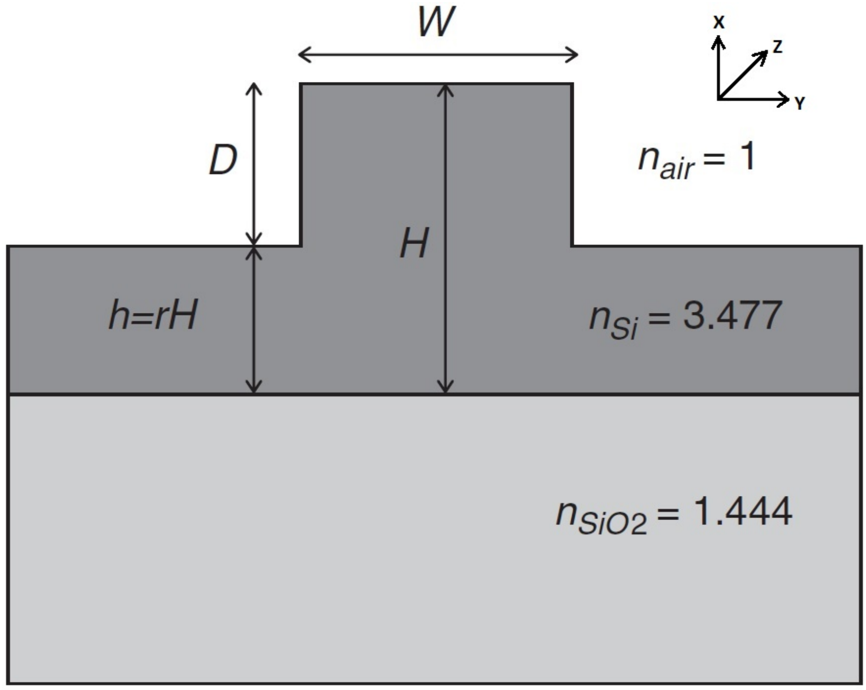

Figure 2.5: Rib waveguide design rules

The main requirements of the waveguide to cater the propagation of waves is that the dimension of the waveguide has to be more than the wavelength of the propagating wave. Depending on the required mode confinement, the width and height are adjusted such that it adheres to 2.5.

- **Design rules of strip waveguides:** In mode confinement of light in optical waveguides the effective mode RI is important. Strip waveguides offer more high RI contrast in comparison to Rib waveguides. This can help in realization of ultra-dense photonic circuits because of high effective mode confinement. This can also achieve small bends which can improve the characterization of different monolithic optical circuits. Sometimes the side walls cannot be etched in a perfectly smooth way causing greater evanescent fields from the waveguides introducing unnecessary coupling and losses. Using simulation for the desired scenario the robust values of the dimensions can be achieved depending on the application.

2.1.3 Snell's law and total internal reflection

If light ray propagating in a medium with RI n_1, impinges on the interface between two media, at an angle θ_1, as shown in Figure 2.6, the ray is partially transmitted (E_t) and partially reflected (E_r). The relationship between the RIs n_1 and n_2, and the angles of incidence (θ_1) and refraction (θ_2), is given by Snell's law:

$$n_1 \sin\theta_1 = n_2 \sin\theta_2 \tag{2.15}$$

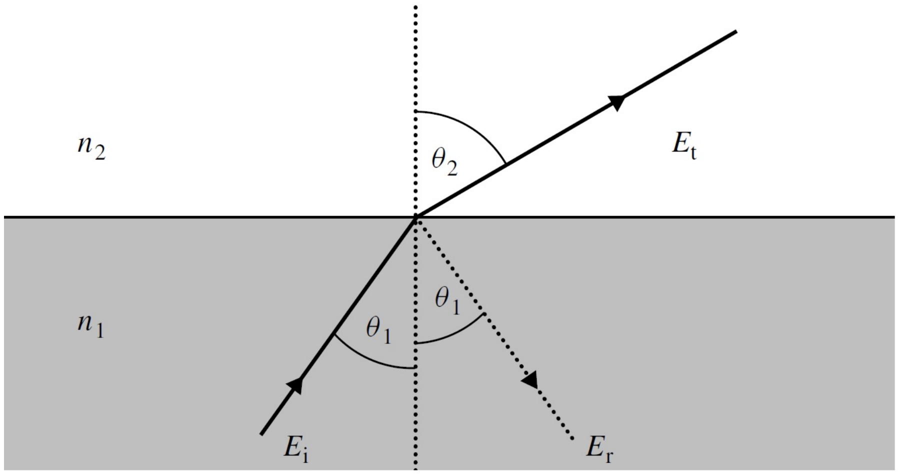

Figure 2.6: Light rays refracted and reflected at the interface of two media

For some angle θ_1, the corresponding angle θ_2 will reach 90°, and hence Snell's law simplifies to:

$$\begin{cases} n_1 \sin\theta_c = n_2 \\ \sin\theta_c = \dfrac{n_2}{n_1} \end{cases} \tag{2.16}$$

where, θ_c is defined as the critical angle. For angles of incidence greater than this critical angle, no light is transmitted and total internal reflection occurs. These properties are important to consider for finding the acceptance angle at which light can be inserted into a waveguide. By enhancing the ray model, a significant understanding of the wave model can be postulated.

2.1.4 Eigenvalue and wave modes

In general, the electric field and magnetic field in the wave equation in 2.8 and 2.11 can be written in its constituent parts in Cartesian coordinates as:

$$\begin{cases} \overrightarrow{E} = E_x\widehat{x} + E_y\widehat{y} + E_z\widehat{z} \\ \overrightarrow{H} = H_x\widehat{x} + H_y\widehat{y} + H_z\widehat{z} \end{cases} \tag{2.17}$$

The generalized vectorial component of the electric and magnetic field of equation 2.13 can be combined into the Helmholtz equation as follows:

$$\nabla^2\Psi\left(x,y,z\right) + k_0^2 n^2\left(x,y\right)\Psi\left(x,y,z\right) = 0 \tag{2.18}$$

where, $\Psi\left(x,y,z\right) = \psi\left(x,y\right)e^{-jkz}$ and then the equation 2.18 can be rewritten as,

$$\nabla_{xy}^2\psi\left(x,y\right) + \left(k_0^2 n^2\left(x,y\right) - k^2\right)\psi\left(x,y\right) = 0. \tag{2.19}$$

The equation 2.19 can be solved for $\psi\left(x,y\right)$, using different numerical analysis methods like FEM, FIT, BPM, FDTD. For optical applications, the main used methods are FEM

(Frequency domain solver), FIT (Time domain solver). The numerical methods first decompose the waveguide into sufficient number small cells (more cells give more robust solution at the cost of increased computing) and then discretization of the refractive index profile is performed. Next the field equations are discretized by replacing the derivatives by their finite difference representations in those cells. In this way a set of linear equations are obtained which can be solved using standard algebraic methods. In general, FIT has a much lower memory footprint.

For given ω, the resulting mode problem is an eigenproblem, solved for eigenvectors, i.e., mode profiles $\psi(x, y)$, and eigenvalues, from which the corresponding propagation constants k of the modes are computed. The geometry of the waveguide is given by the transverse dependence of ϵ, with effective RI profile, and by appropriately chosen boundary conditions. Each allowed solution is referred to as the *mode of propagation*. For example, when light travels through a rectangular waveguide different modes can be visualized as follows in Fig. 2.7.

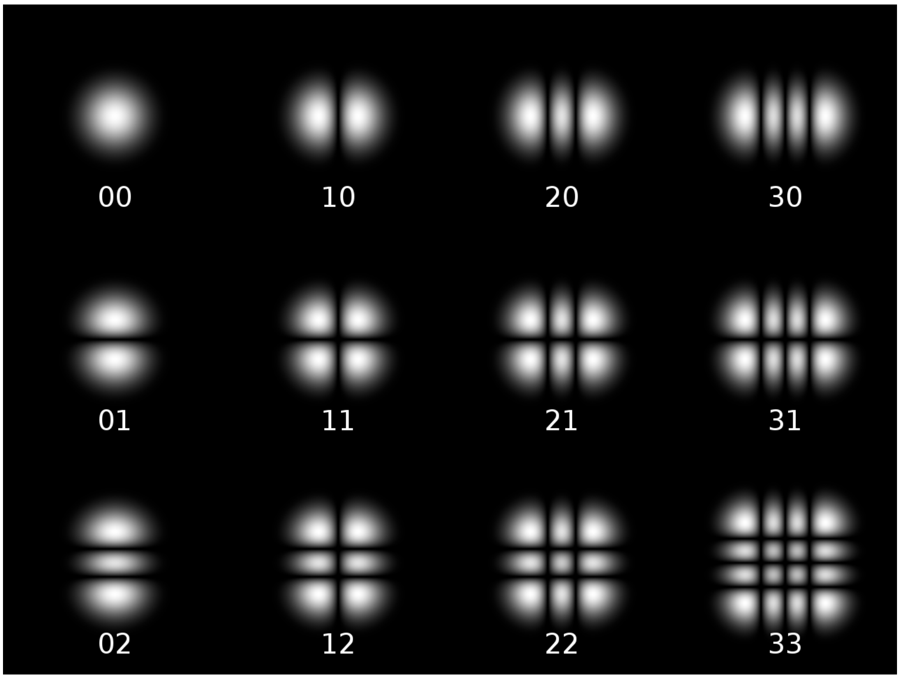

Figure 2.7: Rectangular transverse mode patterns TE(mn)

I will update the picture using CST simulation

2.1.5 Optical polarization and transverse modes

In optical waveguide, the transmission distance is limited by several types of dispersion, or spreading of optical pulses as they travel along the waveguide. Dispersion in waveguide is caused by a variety of factors. Intermodal dispersion, caused by the different axial speeds of different transverse modes, limits the performance of multi-mode waveguide. Because single-mode waveguide supports only one transverse mode, intermodal dispersion is eliminated. In single-mode performance is primarily limited by chromatic dispersion (also called group velocity dispersion), which occurs because the RI of silicon varies slightly depending on the wavelength of the light, and light from real optical transmitters necessarily has nonzero spectral width (due to modulation). PMD, another source of limitation, occurs because although the single-mode waveguide can sustain only one transverse mode, it can carry this mode with two different polarizations, and slight imperfections or distortions in a waveguide can alter the propagation velocities for the two polarizations. This phenomenon is called birefringence and can be counteracted by polarization-rotator. PMD limits the bandwidth of the waveguide because the spreading optical pulse limits the rate that pulses can follow one another on the waveguide and still be distinguishable at the receiver.

Polarization is the direction of the electric field associated with the propagating wave. In the example in Fig. 2.2 the wave is polarized since the electric field and magnetic field exist in one direction only. In a dielectric optical waveguide, light propagates in plane polarized modes and the plane in which light is polarized is either vertical or horizontal to the direction of wave, as shown in Fig. 2.8 in single-mode.

2.1.5.1 TE mode

TE mode is the fundamental mode in which there is no electric field in the direction of propagation of light. In Fig. 2.8 the electric field lines (blue) are perpendicular to the plane of incidence in TE mode. The plane of incidence is the plane in which optical waves strike the surface of the waveguide.

2.1.5.2 TM mode

TM mode is the fundamental mode in which there is no magnetic field in the direction of propagation of light. In Fig. 2.8 it can be seen that magnetic field (red lines) are perpendicular to the plane of incidence in TM mode.

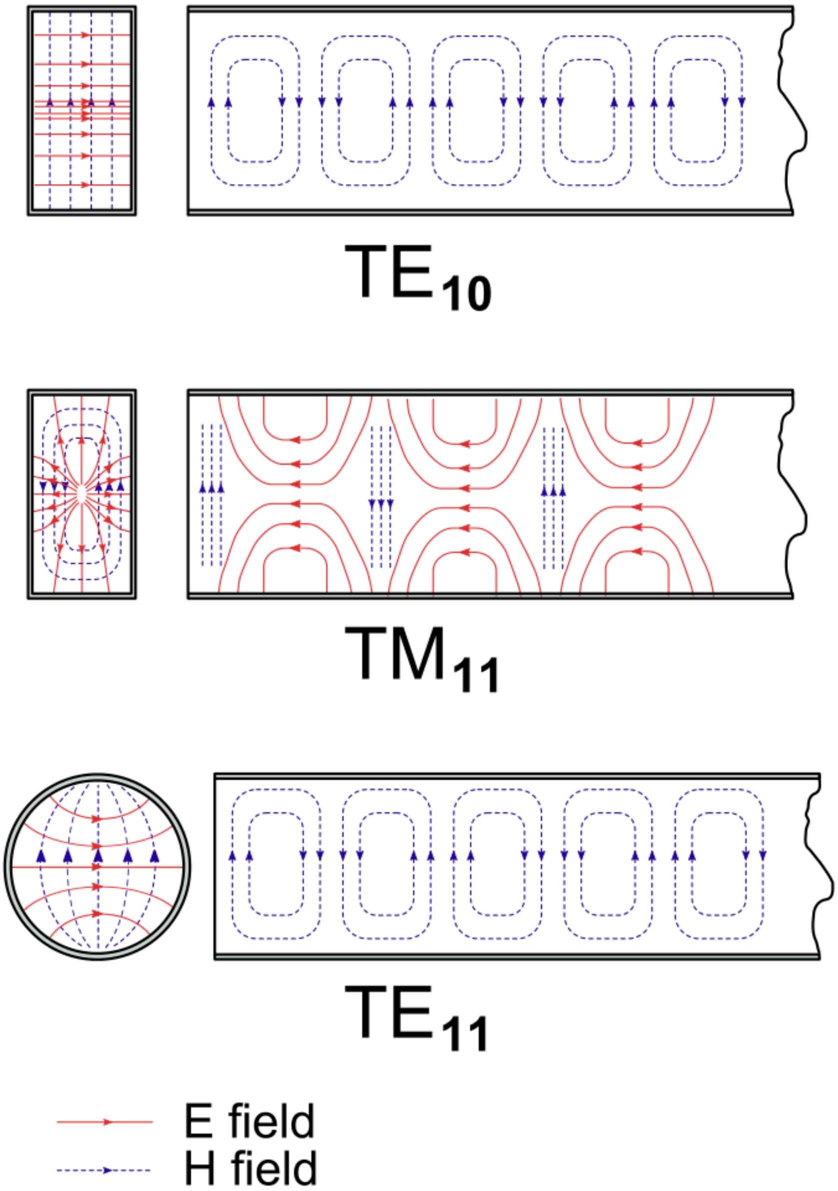

Figure 2.8: TE and TM modes in a waveguide

I will include diagram from my own simulations

2.1.6 Confinement factor

Often it is necessary to know the confined power inside the core of the waveguide which helps in figuring out the waveguide mode. The confinement is also a measure of the proportion of the power in a given mode that lies within the core [40].

$$\text{Confinement factor } = \frac{\int_{-H/2}^{H/2} E_x^2\,(y)\,dy}{\int_{-\infty}^{\infty} E_x^2\,(y)\,dy} \tag{2.20}$$

Confinement factor is an important measure which is function of various factors like polarization, RI difference between the core and cladding, mode number etc.

2.1.7 Jones calculus

Polarized light can be represented using Jones calculus. Polarized light is represented using *Jones vector* and linear optical elements are represented by *Jones matrices.* When light crosses an optical element the resulting polarization of the emerging light is found by taking the product of the Jones matrix of the optical element and the Jones vector of the incident light. *Jones calculus* is only applicable to light that is already fully polarized [41].

2.1.7.1 Jones vector

The Jones vector describes the SOP of light in free space or another homogeneous isotropic non-attenuating medium, where the light can be properly described as transverse waves [41]. The Jones vector is a complex vector that is a mathematical representation of a real wave. A typical representation of the electric field for the optical wave described in 2.8 can be as follows:

$$E = \begin{pmatrix} E_x\,(t) \\ E_y\,(t) \\ 0 \end{pmatrix} = \begin{pmatrix} E_x e^{i(\omega t - kz + \phi_x)} \\ E_y e^{i(\omega t - kz + \phi_y)} \\ 0 \end{pmatrix} = \begin{pmatrix} E_x e^{i\phi_x} \\ E_y e^{i\phi_y} \\ 0 \end{pmatrix} e^{i(\omega t - kz)} \tag{2.21}$$

where ϕ_x and ϕ_y indicate the phasor notation. The Jones vector of the plane wave is described by:

$$\begin{pmatrix} E_x e^{i\phi_x} \\ E_y e^{i\phi_y} \end{pmatrix} \tag{2.22}$$

and the intensity of the optical, I wave can be written as,

$$I = |E_x|^2 + |E_y|^2 \tag{2.23}$$

Generally, when considering Jones vector a wave of unit intensity is required for the consideration polarization, so Jones vector is noted using an unit vector where,

$$E\overline{E} = 1 \tag{2.24}$$

where $\overline{E}$ is the complex conjugate of E. In general the Jones representation of a normalized elliptically polarized beam with azimuth θ and elliptical angle ϵ is given by,

$$e^{i\phi} \begin{pmatrix} \cos\theta\cos\epsilon - j\sin\theta\sin\epsilon \\ \sin\theta\cos\epsilon - j\cos\theta\sin\epsilon \end{pmatrix} \tag{2.25}$$

where $e^{i\phi}$ is an arbitrary phase vector and $\phi = \phi_x - \phi_y$. So, for example a linear polarization of TE mode can be represented as,

$$\begin{pmatrix} 1 \\ 0 \end{pmatrix} \tag{2.26}$$

since, $\theta = 0$ and $\epsilon = 0$.

2.1.7.2 Jones matrix

Jones matrix are the formal representation of the various optical elements such as lenses, beam splitters, mirrors, phase retarders, polarizers at arbitrary angles that can modify polarization. They generally operate on Jones vector and helps in comprehend situations which light encounters multiple polarization elements in sequence. In these situations the products of the Jones matrices can be used to represent the transfer matrix. This situation can be represented using,

$$[E_{output}] = J_{system}[E_{input}] \tag{2.27}$$

where E_{input} is the input field into the optical system and E_{output} is the generated output field represented using Jones vector. The matrix J_{system} is the Jones matrix of the optical system comprising of a series of polarization devices. If there are N devices in the system then the final transfer matrix comes out as,

$$J_{system} = J_N J_{N-1} \ldots\ldots J_2 J_1 \tag{2.28}$$

where J_N is the Jones matrix for n^{th} polarizing optical element.

2.1.8 Jones matrix for polarizing optical systems

To construct optical waveguides for polarization rotation it is imperative to deal with the basic principles of standard available optical systems. Here, the fundamental principles of polarizer and wave plates are interpreted using Jones calculus.

2.1.8.1 Polarizer

Polarizers have an index of refraction which depends on orientation electric field propagation. If any optical system has a transmission axis and an absorption axis for electric fields, then lights will be passed along he transmission axis and absorbed along the other axis. So, the Jones matrix of a polarizer making an angle θ with the X-axis will come out as,

$$\begin{pmatrix} \cos^2\theta & \sin\theta\cos\theta \\ \sin\theta\cos\theta & \sin^2\theta \end{pmatrix} \tag{2.29}$$

2.1.8.2 Wave plates

Wave plates are phase retarders which are made of birefringent crystals. Wave plates can be conceptualized as two polarizers kept apart at certain distance d, such that their polarization axes are apart orthogonally (90^0). The phase difference as light passes through this setup of thickness d is,

$$(k_{slow} - k_{fast})\, d = \frac{2\pi d}{\lambda_{vac}} (n_{slow} - n_{fast}) \tag{2.30}$$

In, general the Jones matrix for a wave plate is given by,

$$\begin{pmatrix} \cos^2\theta + \xi \sin^2\theta & \sin\theta\cos\theta - \xi \sin\theta\cos\theta \\ \sin\theta\cos\theta - \xi \sin\theta\cos\theta & \sin^2\theta + \xi \cos^2\theta \end{pmatrix} \tag{2.31}$$

where ξ is calculated based on the type of wave plate. The following equations addresses some general scenarios:

$$\begin{cases} \xi = e^{i\pi/2}, & \text{where, } (k_{slow} - k_{fast})\, d = \pi/2 + 2\pi m, \text{for quarter-wave plate} \\ \xi = e^{i\pi}, & \text{where, } (k_{slow} - k_{fast})\, d = \pi + 2\pi m, \text{for half-wave plate} \end{cases} \tag{2.32}$$

Similar concept is used in the construction of PR waveguides which will be discussed in later sections shortly.

2.1.9 Poincaré sphere and state of polarization

To view a complete representation of all the polarization ellipses generated using Jones vectors, a spherical structure with unit radius is used, which is known as Poincaré sphere. If the orientation in space of of the ellipse of polarization is determined by the azimuth, θ and ellipticity, ϵ then that point can be completely characterized by its longitude 2θ and latitude 2ϵ. The north and south poles represent the right-handed and left-handed circular polarization respectively. In general the diametrically opposite points represent pairs of orthogonal polarization. The SOP and its corresponding location in the Poincaré sphere is visualized in the Fig. 2.9. To go from one SOP to another the polarized light can be passed through various optical components which can be computed using the Jones matrix and the corresponding SOP can be depicted on the Poincaré sphere as well.

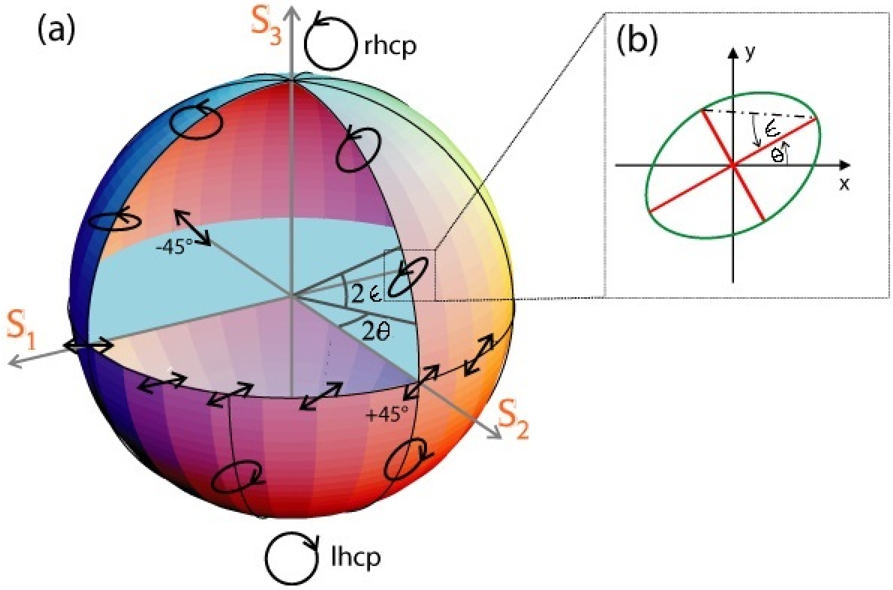

Figure 2.9: (a) Representation of the Poincaré sphere (b) Representation of the ellipse parameters [42]

The SOP of any wave is also defined using Polarization extinction ratio (PER) and polarization phase, ϕ given by the following equations:

$$\begin{cases} PER_{TE-TM} = 10\log\dfrac{P_{TM}}{P_{TE}} \\ PER_{TM-TE} = 10\log\dfrac{P_{TE}}{P_{TM}} \\ \phi = \phi_x - \phi_y \end{cases} \tag{2.33}$$

For complete polarized light, the point on the Poincaré sphere must be fixed on time which requires,

$$\frac{E_x(t)}{E_y(t)} = constant \tag{2.34}$$

and,

$$\phi = \phi_x(t) - \phi_y(t) = constant \tag{2.35}$$

2.1.10 Stoke's parameter

Quasi-monochromatic waves are mathematically treated using Stokes parameters (S_0, S_1, S_2, S_3), which constitute a vector generally known as Stokes vectors. Stokes vectors are used to keep track of the partial polarization (and attenuation) of a light beam in terms of total intensity (I), degree of polarization (p) and ellipse parameters, as the light progresses through an optical system. A Stokes vector can generally be represented as,

$$\overrightarrow{S} = \begin{pmatrix} S_0 \\ S_1 \\ S_2 \\ S_3 \end{pmatrix} \tag{2.36}$$

where,

$$\begin{cases} S_0 = I \\ S_1 = I_p \cos 2\theta \cos 2\epsilon \\ S_2 = I_p \sin 2\theta \cos 2\epsilon \\ S_3 = I_p \sin 2\epsilon \end{cases} \tag{2.37}$$

Here, $I_p, 2\theta, 2\epsilon$ are the spherical coordinates of the 3-D vector of Cartesian coordinates (S_1, S_2, S_3). So, given the Stokes parameters, the spherical coordinates $(p, 2\theta, 2\epsilon)$ can be obtained and represented by a point inside the Poincaré sphere using the following:

$$\begin{cases} I = S_0 \\ p = \dfrac{\sqrt{S_1^2 + S_2^2 + S_3^2}}{S_0} \\ 2\theta = \tan^{-1} \dfrac{S_2}{S_1} \\ 2\epsilon = \tan^{-1} \dfrac{S_3}{\sqrt{S_1^2 + S_2^2}} \end{cases} \tag{2.38}$$

The prescribed notations are portrayed on the Poincaré sphere in the following Fig. 2.10.

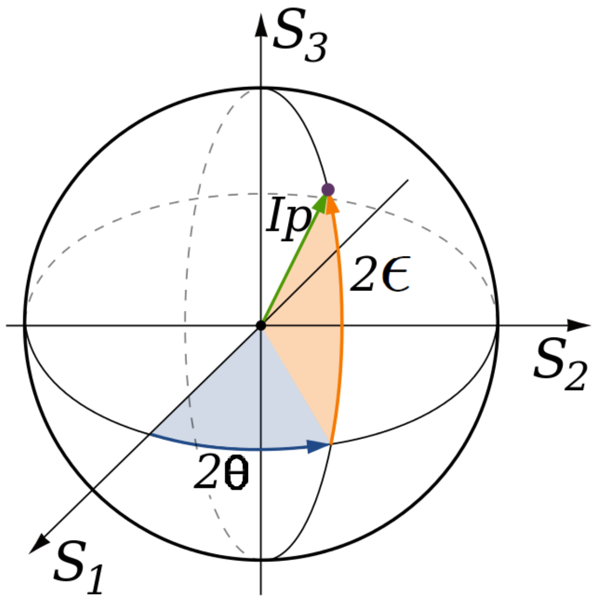

Figure 2.10: Poincaré sphere, on or beneath which the three Stokes parameters [S1, S2, S3] are plotted in Cartesian coordinates [43]

2.1.11 Coupling mode theory

In a waveguide, an ideal mode is an eigenvector of a propagation constant. Mode coupling enables transfer of energy from one ideal mode to another, during propagation. Mode coupling can be induced by introducing randomness in the waveguide. This can be achieved through random or intentional index perturbations, bends and stresses within a waveguide, or by introducing another independent waveguide structure in close proximity (coupled waveguides in close proximity are modeled as a single structure, forming supermodes). The pairwise coupling strength between two modes depends on a dimensionless ratio between the coupling coefficient (per unit length) and the difference between the two modal propagation constants. Hence, a given perturbation may strongly couple modes having nearly equal propagation constants, but weakly couple modes having highly unequal propagation constants. PMD and PDL have long been described by field coupling models, in which phase dependent coupling of modal fields is described by complex coefficients. Field coupling models describe not only a redistribution of energy among modes, but also how eigenvectors and their eigenvalues depend on the mode coupling coefficients [44].

Perturbation Analysis: Supermodes can be represented as weighted sum of individual guided modes. If two modes are represented by $\psi_1(x, y)$ and $\psi_2(x, y)$ in the different waveguides along with the coupling between two modes as $X_i(z)$, then the supermode can be written using Helmholtz identity as,

$$\Psi(x, y, z) = X_1(z)\psi_1(x, y) + X_2(z)\psi_2(x, y) \tag{2.39}$$

The uncoupled modes, ψ_1 and ψ_2 satisfy the following propagation equations with propagation constants k_1 and k_2,

$$\begin{cases} \dfrac{dX_1}{dz} = -jk_1X_1 \\ \dfrac{dX_2}{dz} = -jk_2X_2 \end{cases} \tag{2.40}$$

A known solution for 2.40 is:

$$\begin{cases} X_1(z) = e^{-jk_1z} \\ X_2(z) = e^{-jk_2z} \end{cases} \tag{2.41}$$

Coupled mode theory postulates that to describe a perturbed system the linear coupling terms need to be added as,

$$\begin{cases} \dfrac{dX_1}{dz} = -jk_1X_1(z) - j(\kappa_{11}X_1 + \kappa_{12}X_2) \\ \dfrac{dX_2}{dz} = -jk_2X_2(z) - j(\kappa_{21}X_1 + \kappa_{22}X_2) \end{cases} \tag{2.42}$$

where, κ_{ij}, $\forall\,(i, j) \in [1, 2]$ are the linear coefficients which can be understood using the scattering matrix as,

$$\begin{pmatrix} \kappa_{11} & \kappa_{12} \\ \kappa_{21} & \kappa_{22} \end{pmatrix} \tag{2.43}$$

where,

$$\begin{cases} \kappa_{11} = \dfrac{1}{2}k_0^2 \int\int (n_{12}^2 - n_1^2)\psi_1^2 dxdy \\ \kappa_{12} = \dfrac{1}{2}k_0^2 \int\int (n_{12}^2 - n_1^2)\psi_1\psi_2 dxdy \\ \kappa_{21} = \dfrac{1}{2}k_0^2 \int\int (n_{12}^2 - n_2^2)\psi_1\psi_2 dxdy \\ \kappa_{22} = \dfrac{1}{2}k_0^2 \int\int (n_{12}^2 - n_2^2)\psi_2^2 dxdy \end{cases} \tag{2.44}$$

Here, κ_{11} and κ_{22} are the reflection coefficients and κ_{12} and κ_{21} are the coupling coefficients. Normally, it is assumed that the modes are normalized, and propagate in a lossless system with symmetric coupling coefficients. Hence,

$$\kappa_{12} = \kappa_{21} \tag{2.45}$$

Coupling coefficients and phase mismatch are important factors for power exchange between different modes. In 2.11a both the waveguides are excited where as in 2.11b only waveguide B is excited.

Change this pic with some other diagram or simulations..

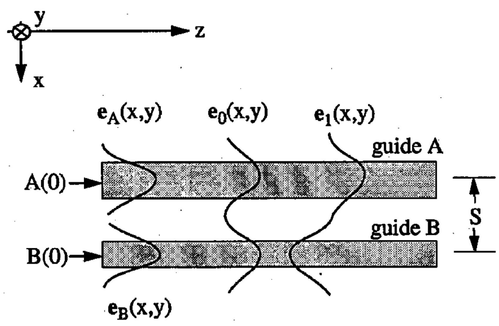

(a) Individual and normal modes in two different waveguides

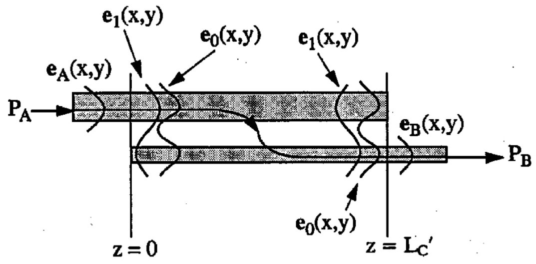

(b) Power transfer from arm A to arm B by normal-mode coupling

Figure 2.11: Description of the directional coupler under coupled-mode and normal-mode

In 2.11b for no phase mismatch complete power exchange occurs. This is why phase matching is an important criteria for mode coupling. The coupling length, $L_c = \pi/2\kappa$.

Coupling mode theory has been successfully applied to the modeling and analysis of various guided-wave optoelectronic devices, such as optical directional couplers made of thin film and channel waveguides, multiple waveguide lenses, phase-locked laser arrays, distributed feedback lasers and distributed Bragg reflectors, grating waveguides and couplers, nonparallel and tapered waveguide structures, Y-branch waveguides, TE/TM polarization converters, mode conversion and radiation loss in slab waveguides, residual coupling among scalar modes. It has also been used to study the wave coupling phenomena in nonlinear media such as harmonic generation in bulk and guided-wave devices, and nonlinear coherent couplers [45].

2.2 Polarization tuning in optical waveguide

Should this section be written in context of polarization tuning? Should it go after PR?

2.2.1 Thermo-optic mechanism

Mach-Zehnder...??

Is it there?..chec

2.2.2 Electro-optic mechanism

Mach-Zehnder...?

Is it there?..chec

2.2.3 Liquid crystals

2.2.4 Current injection

2.2.5 MEMS

Actuation principle...

Why is MEMS better?

2.3 Polarization rotator (PR)

For an overall robust network, PRs are necessary in optical fiber and OEIC, which are realized in different approach.

2.3.1 Optical fiber PR

Check here..Industry standards..

Write about the PR in optical fiber short with industry standards..

2.3.2 On-chip PR

The currently available OEIC PRs can be classified under two categories as passive and active PR. In the passive PRs the waveguide structures are designed in a specific way to manipulate the effective RI of the waveguide, in order to obtain the desired polarization. The RI cannot be manipulated or tuned once fabricated. Whereas, in active PRs, the effective RI can be manipulated by thermo-optic or quantum effects.

2.3.2.1 Passive PR

The fields in TE and TM mode do not couple with each other and are of different symmetry. Thus asymmetric structure in both horizontal and vertical directions are required to break the symmetry which are accomplished using different principles viz. mode coupling [32, 46, 31], mode evolution [47, 34, 48, 49, 50] and mode hybridization [51, 30, 52, 29], described in the following sections. All these principles are based on the coupling mode theory described in 2.1.11.

I am not sure how to approach this section

Mode coupling: Mode coupling PR includes a pair of waveguide core layers running parallel to each other, within close proximity. When two modes with orthogonal polarizations have equal effective RIs, strong mode coupling occurs in the waveguide, and with proper taper orientation and design, length of coupling region, one mode can be effectively converted to the other.

☐ **Design: Ultra-compact polarization splitter-rotator based on silicon nanowires**

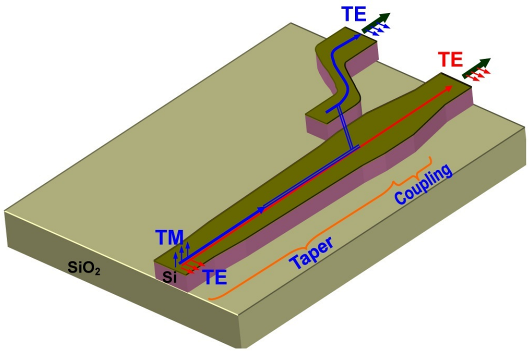

(a) Schematic of the PR

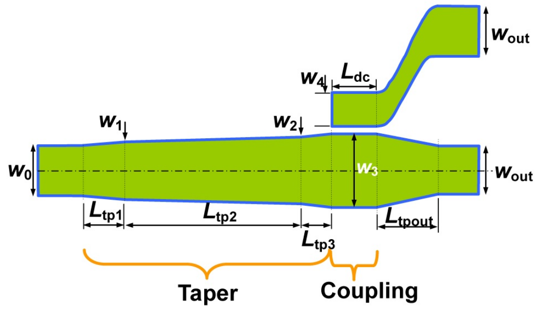

(b) Structure of the PR

Figure 2.12: PR using mode coupling, by Dai and Bowers [32]

The coupler (Fig. 2.12a) consists of 2 waveguides parallel to each other. The section where coupling occurs is shown in Fig. 2.12b. The taper structure is singlemode at the input end (W_0) while it becomes multimode at the other end (W_3). When light propagates along the taper structure, the TM fundamental mode launched at the narrow end (W_0) is converted to the first higher-order TE mode at the wide end (w_3) because of the mode coupling between them. Another narrow optical waveguide (W_4) is then place close to the wide waveguide (W_3) and an asymmetrical directional coupler is formed. By using this asymmetrical directional coupler, the first higher-order TE mode in the wide waveguide is then coupled to the TE fundamental mode of the adjacent narrow waveguide. In this way, the input TM fundamental mode at the input waveguide is finally converted into the TE fundamental mode at the cross port of asymmetrical directional coupler. On the other hand, the input TE polarization keeps the same polarization state when it goes through the adiabatic taper structure. In the region of the asymmetrical directional coupler, the TE fundamental mode in the wide waveguide could not be coupled to the adjacent narrow waveguide because of the phase mismatching. In this way, TE- and TM- polarized light are separated while the TM fundamental mode is also converted into TE fundamental mode [32].

Various other designs for mode coupling have also been proposed [31, 46], which work on the same principle.

☐ **Problem of mode coupling:** Due to the large birefringence of silicon waveguides, the conversion usually occurs between fundamental TM and high order TE modes and subsequently the high order TE mode is converted to the fundamental TE mode.

Mode evolution: The mode evolution based PR includes a pair of waveguide core layers. The waveguide is designed in such a way that the cross section of the waveguide varies along the direction of propagation. This changes polarization from TE to TM or vice versa gradually in propagation direction, under adiabatic transition conditions.

☐ **Design A: Mode evolution PR based on single taper**

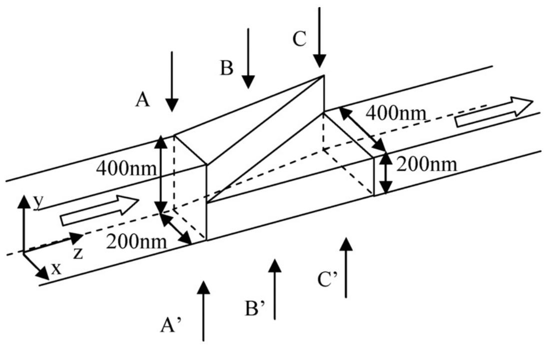

(a) Schematic of the PR

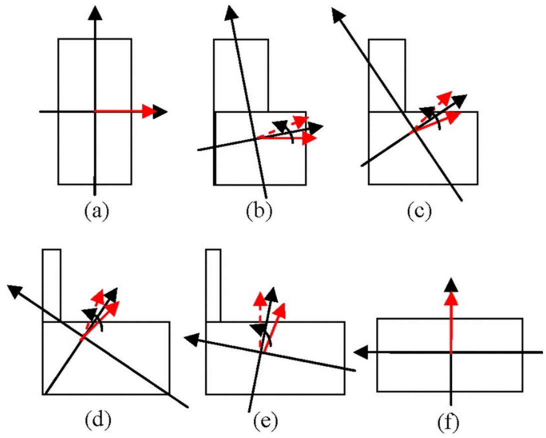

(b) Cross sections of the waveguide at A-A'(a), B-B'(c), and C-C'(f) along with the transition states of the polarization

Figure 2.13: PR using mode evolution, by Zhang *et al.* [47]

The PR (Fig. 2.13a) consists of the variable cross section for polarization rotation. The transition region of the rotator was divided into N sections. Each section was considered as a uniform asymmetrical waveguide like the rotator in [53]. The length of each section was its half-beat length. The half-beat length of the n^{th} section is $L_{\pi}^{n} = \left(\pi / \left(\beta_1^n - \beta_2^n\right)\right)$, where $\beta^n = (2\pi/\lambda)\, n_{eff}^n$ and β_1^n and β_2^n are the propagation constants of the two fundamental modes in the n^{th} section. After propagating in the n^{th} section, the polarization will rotate $2\Delta\varphi_n$ toward the optical axis, where φ_n is the angle between the optical axis and the polarization of the incident light. The overall rotator should satisfy $\sum_n 2\Delta\varphi_n = 90^0$, to achieve a rotation of 90^0 in the cascaded sections. Fig. 2.13b shows the rotation procedure [47].

□ **Design B: Mode evolution PR composed of an asymmetric-rib waveguide and a tapered waveguide**

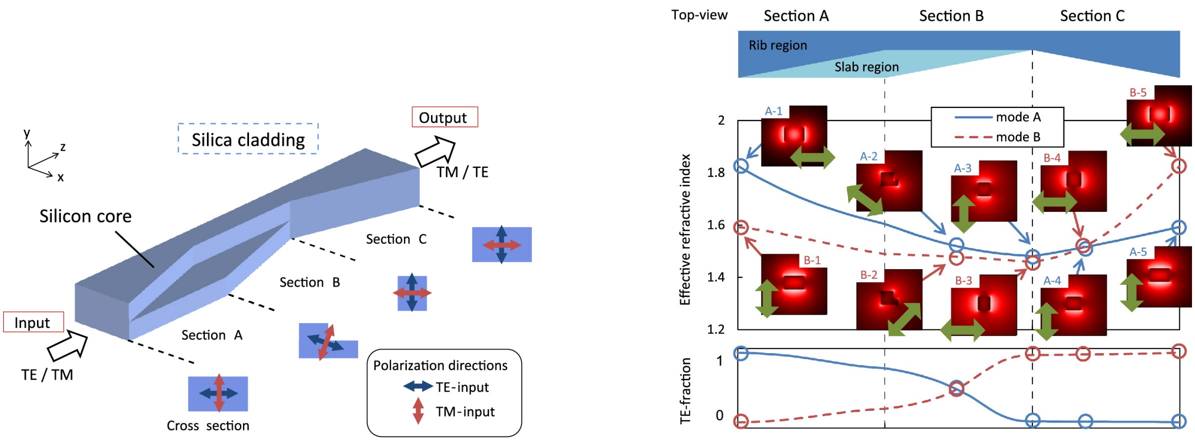

(a) Schematic of the PR

(b) Local mode analysis of the PR

Figure 2.14: PR using mode evolution, by Goi *et al.* [50]

The PR (Fig. 2.14a) consists of the polarization rotation sections(A and B) with an asymmetric rib waveguide and the mode size conversion section(C) with a nano-tapered waveguide. This design provides both vertical and horizontal asymmetry.

Apart from these, other designs for mode evolution have also been proposed [34, 48, 49], which has the same basic principle.

□ **Problem of mode evolution:** In mode evolution, silicon waveguide is top-clad with a Si or SiN material with specially designed tapers to enable gradual mode conversion between orthogonal polarization states. This kind of top-cladding increases the complexity of fabrication and sharp tips at the end of tapers necessary for low conversion loss are also difficult to make. A pure silicon solution is proposed in [47], but in their structure the input and output silicon waveguides have different thicknesses. The structure in [50] solves this problem at the cost of a longer device length of 230µm.

Mode hybridization: Mode hybridization works by breaking the symmetry of the silicon waveguide cross section. The propagation modes are hybridized due to introduced asymmetry, allowing optical power to be transferred periodically between the two desired polarization states. The rotation is essentially enabled through interference of the two hybridized modes.

□ **Design A: Asymmetric silicon nanowire waveguide as compact PR**

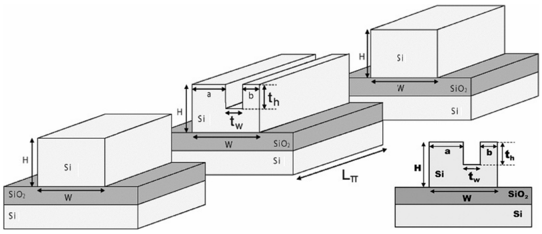

(a) Schematic diagram of the asymmetric PR

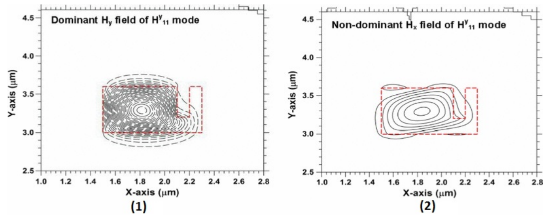

(b) Contour plots of (1) the dominant H_y field profile and (2) the non-dominant H_x field profile of the H^y_{11} mode with W = 800nm and H = 800nm, t_w = 100nm and t_h = 400nm

Figure 2.15: PR using mode hybridization, by Leung *et al.* [30]

Fig. 2.15a depicts the single-stage polarization rotator, which consists of two Si strip waveguides with straight sidewalls, where both are butt coupled to an Si asymmetric strip polarization rotator waveguide in the middle. In the design of a polarization rotator, an asymmetric section which supports the highly hybrid modes is sandwiched between two standard Si waveguides where the hybridness is small. When a quasi-TE (or quasi-TM) mode from a standard Si waveguide with its polarization angle at nearly zero degrees (or indeed 90°) is launched into the asymmetric section (which supports highly hybrid modes with polarization direction ±45°), then both of them are excited almost equally to satisfy the continuity of the E_t and H_t fields at that interface. These two highly hybrid modes travel along the asymmetric sections. The half-beat length is a key parameter used in order to identify the optimum length of this asymmetrical section to achieve the maximum polarization rotation. The half-beat length is defined as $L_\pi = \pi/\Delta\beta$, where $\Delta\beta$ is the difference between the propagation constants of the H^x_{11} and the H^y_{11} modes. After propagating a distance $L = L_\pi$, the original phase condition between the highly polarized modes would be reversed, and the polarization state of the superimposed modes would be rotated by 90°. If a standard Si waveguide (with smaller modal hybridness) is placed at this position, this quasi-TM (or quasi-TE) mode would propagate without any further polarization rotation [30].

□ **Design B: Efficient silicon PR based on mode-hybridization in a double-stair waveguide**

The PR [28], based on a double-stair silicon waveguide fabricated with three etch steps as described in Fig.2.16a is better compared to the two-etch-step structure with single-stair cross section [54] because of higher PER and a broader optical bandwidth.

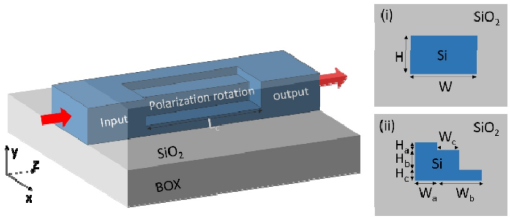

(a) Schematic structure of the double-stair PR. Inset shows the cross-section

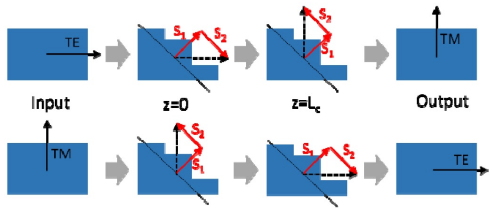

(b) Polarization rotation process along the waveguide. The arrows indicate the direction of mode electric field. $Z = 0$ is the starting position of the polarization rotation section

Figure 2.16: PR using double-stair waveguide mode hybridization, by Xie *et al.* [28]

The schematics of the PR (Fig. 2.16a) consists of the polarization rotation sections and describes the mode conversion along the waveguide.

Other designs for mode hybridization have also been proposed [51, 52], which work on same principle.

- ☐ **Problem of mode hybridization:** The narrow trenches (∼10 nm wide) required for mode hybridization are difficult to pattern and etch with controllable profiles. Recently, a PR [54] is realized on a simple strip waveguide by cutting one upper corner of the waveguide in a two-step etch process following the original idea in [53]. The pure silicon solution [54], without the need of extra materials is quite attractive, but the measured PER is relatively low around ∼6 dB within a ∼30 nm bandwidth. Although, the double-stair waveguide [28], offers good results but still the PER is not tunable. They rotate polarization only by a fixed amount and exhibit wavelength-dependent loss because its working principle relies on periodic structures.

2.3.2.2 Active PR

An active PR is generally achieved by multiple tunable controllers which gives a good trade-off between integration and performance.

Tunable polarization controller with thermo-optic effect: The PRs mainly change the PER, whereas the Tunable polarization phase shifters (TPPS) control the polarization phase. The TPPS is implemented using waveguide heaters placed alongside, the waveguide with little spacing, to avoid losses due to interaction of the evanescent field with the metal. The waveguide heaters are electrically tunable.

☐ **Design: Tunable PR with phase shifters**

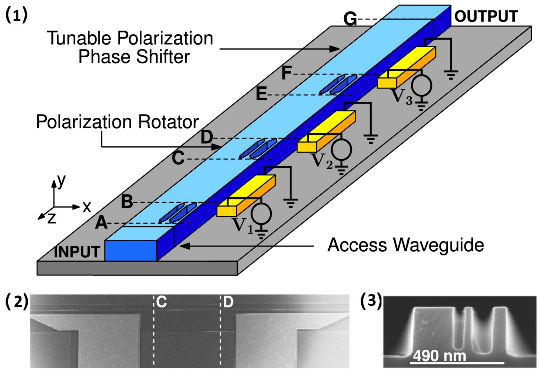

(a) Schematic of the polarization controller along with the cross section of the PR, which uses mode hybridization. The cross section of mode hybridization PR can be seen in (3)

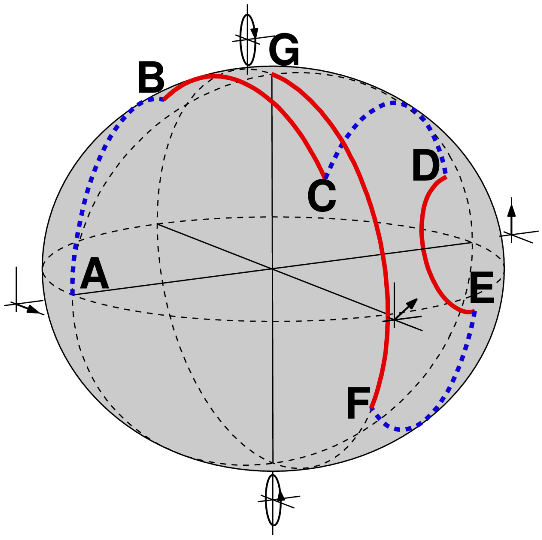

(b) Evolution of SOP throughout the device

Figure 2.17: PR control using three PR and three TPPS, by Merenguel *et al.* [35]

In the passive PRs, the individual PR had to produce an exact polarization conversion. This was overcome by the design of the PR in Fig. 2.17a. The PR (Fig. 2.17a) consists of three PRs and three TPPS which control the SOP. The operation of the device is illustrated in Fig. 2.17b using the Poincaré sphere 2.1.9. First, a certain PR will be performed in the first PR (point B). Following the first PR there are two pairs of TPPS–PR. Each TPPS will tune the polarization phase in order to feed the PRs with the suitable polarization phase so that, at the output of the third PR (point F), the desired PER is achieved. The last TPPS then produces the appropriate polarization phase shift so that the desired SOP is obtained at the output (point G).

☐ **Drawbacks of polarization controller with thermo-optic effect:** Although, the design offers good trade-off between performance and size but still it is limited that by the fact that thermal effect can induce phase in other waveguides due to cross-talk. This may occur when this system is used in commercial designs with high packing density.

Tunable polarization controller using Berry's phase: Berry's phase is a quantum-mechanical phenomenon that may be observed at the macroscopic optical level through the use of an enormous number of photons in a single coherent state [55]. In the special case of planar (non-helical) paths, such as the paths typically taken by planar optical waveguides, no significant optical rotation is observed independent of the complexity of the path [56]. The key to manifest Berry's phase in photonic integrated circuits is to introduce out-of-plane three-dimensional waveguides to create a two-dimensional momentum space with non-zero (Gaussian) curvature.

- ☐ **Design: Tunable PR with Berry's phase**

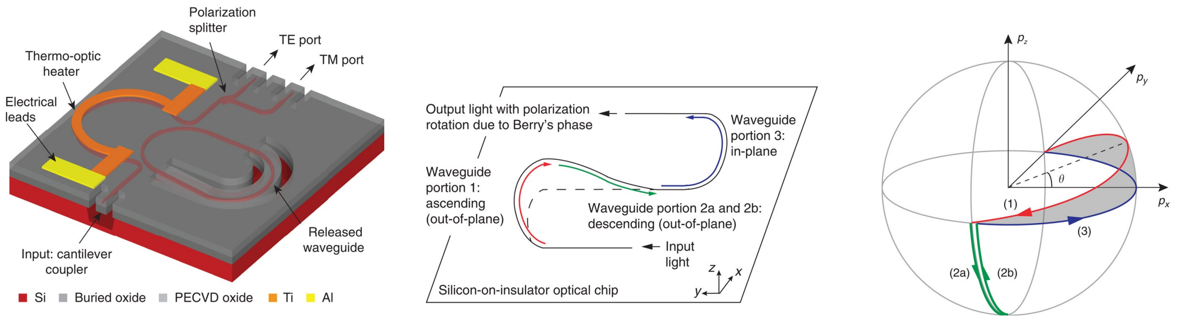

(a) Schematic of the device (b) Layout of device involving out-of-plane waveguides (c) Evolution of SOP throughout the device

Figure 2.18: PR control using three PR and three TPPS, by Xu *et al.* [37]

Monochromatic light at wavelength λ carries a momentum given by $p = p_x\hat{x} + p_y\hat{y} + p_z\hat{z} = \hbar k$, where k is the propagation vector, with magnitude $2\pi/\lambda$ and $\hbar$ is the Planck's constant divided by 2π. In physical space, the layout consists of three main portions. The first portion, shown in red in Fig. 2.18b, consists of an ascending out-of-plane 180° waveguide bend. The second portion, shown in green, consists of an out-of-plane waveguide that descends to the chip surface. Finally, the third portion consists of an in-plane 180° bend. In momentum space, the corresponding paths for each waveguide portion are shown in Fig. 2.18c using Poincaré sphere (2.1.9). Light propagation along the three-dimensional path in physical space results in a non-zero subtended solid angle in momentum space, shown as the shaded area in Fig. 2.18c. Therefore, the waveguide geometry will exhibit Berry's phase. A change in wavelength results in a change of the radius of the sphere in momentum space but not the solid angle. If the deflection angle of waveguide portion 1, in the physical space shown in Fig. 2.18b is θ, then the output light will appear with polarization rotation equal to 2θ due to Berry's phase because the magnitude of the solid angle extended by the grey area in momentum space, shown in Fig. 2.18c, is θ [37].

- ☐ **Drawbacks of polarization controller with Berry's phase:** This device uses out-of-plane ring cavity which uses the principles of ring resonator. The ring resonator is limited by its narrow band spectral features which limits bandwidth.

3 Chapter 3
Design and simulation

3.1 Approach

Say standard mode solver softwares like Comsol, CST [57] can be used to solve the modes in equation 2.19

How this section can be writ- ten?

update here...

3.2 Designing the experiment

3.2.1 Design principle

3.2.2 Design A:

3.2.3 Design B:

3.2.4 Design C:

3.3 Choice of simulation

3.4 Simulation results and analysis

Chapter 4

4 Fabrication

Fabrication example followed from here [58]

Chapter 5

5 Interpreting the results

5.1 Experimental setup for measurement

5.2 Results

5.3 Analysis

Chapter 6

6 Discussion

6.1 Limitations

6.2 Future work

Chapter 7

7 Conclusions

Todo list

Less than copper...verify 2
I will update the picture using CST simulation 13
I will include diagram from my own simulations 15
Change this pic with some other diagram or simulations.. 22
Should this section be written in context of polarization tuning? Should it go after PR? 23
Is it there?..check 23
Is it there?..check 23
Why is MEMS better? 23
Write about the PR in optical fiber short with industry standards.. 23
I am not sure how to approach this section 23
How this section can be written? 31
update here... 31

Abbreviations

BPM Beam propagation method. 10, 12

CAGR Compound annual growth rate. 4

CMOS Complementary metal-oxide semiconductor. 3, 4

EM Electromagnetic. 2, 6–8

FDTD Finite difference time domain. 10, 12

FEM Finite element method. 10, 12

FIT Finite integration technique. 10, 12, 13

IC Integrated circuit(s). 3

ICT Information and communication technology. 2

IMS IP Multimedia Subsystem. 2

IoT Internet of Things. 1

MEMS Microelectromechanical systems. 4, 5

OEIC Optoelectronic integrated circuit. 3, 4, 23

PDλ Polarization dependent wavelength characteristics. 4

PDL Polarization dependent loss. 4, 21

PER Polarization extinction ratio. 19, 27–29

PMD Polarization mode dispersion. 4, 14, 21

PR Polarization rotator. 4–6, 18, 23–30

RI Refractive index. 4, 8, 9, 11, 13, 14, 16, 23, 24

SMC Single-mode condition. 10

SOP State of polarization. 6, 16, 18, 19, 29, 30

TE Transverse Electric. 9, 10, 13–15, 17, 22–25, 27

TEM Tansverse Electromagnetic. 8

TM Transverse Magnetic. 9, 10, 14, 15, 22–25, 27

TPPS Tunable polarization phase shifters. 28–30

TPR Tunable polarization rotator. 4, 5

Bibliography

[1] "Gartner says the internet of things installed base will grow to 26 billion units by 2020." http://www.gartner.com/newsroom/id/2636073, 2013. [Online; accessed 26-Jan-2016].

[2] "Ericsson Mobility Report: 70 percent of world's population using smartphones by 2020." http://www.ericsson.com/news/1925907, 2015. [Online; accessed 06-Feb-2016].

[3] "Number of Internet Users (2015) - Internet Live Stats." http://www.internetlivestats.com/internet-users/, 2015. [Online; accessed 22-Jan-2016].

[4] "Ericsson traffic exploration infograph." http://www.ericsson.com/TET/trafficView/loadBasicEditor.ericsson, 2015. [Online; accessed 06-Feb-2016].

[5] "What Happens in an Internet Minute [Infographic] | Daily Infographic." http://www.dailyinfographic.com/what-happens-in-an-internet-minute-infographic, 2013. [Online; accessed 29-Jan-2016].

[6] "Silicon photonics." https://en.wikipedia.org/wiki/Silicon_photonics/, 2015. [Online; accessed 06-Feb-2016].

[7] "ARK | Your Source for Intel® Product Specifications." http://ark.intel.com/, 2015. [Online; accessed 06-Feb-2016].

[8] "Cisco Global Cloud Index: Forecast and Methodology, 2014–2019 White Paper." http://cisco.com/c/en/us/solutions/collateral/service-provider/global-cloud-index-gci/Cloud_Index_White_Paper.html. [Online; accessed 04-Feb-2016].

[9] G. Reed and A. Knights, *Silicon Photonics: An Introduction.* Wiley, 2004.

[10] N. Savage, "Linking Chips With Light." http://spectrum.ieee.org/semiconductors/optoelectronics/linking-chips-with-light, 2015. [Online; accessed 06-Feb-2016].

[11] R. Stabile, A. Albores-Mejia, A. Rohit, and K. A. Williams, "Integrated optical switch matrices for packet data networks," *Microsystems & Nanoengineering*, vol. 2, p. 15042, Jan. 2016.

[12] M. C. Wu, T. J. Seok, S. Han, and N. Quack, "MEMS-Enabled Scalable Silicon Photonic Switches," *Optics Letters*, p. FW3B.2, 2015.

[13] D. Nikolova, S. Rumley, D. Calhoun, Q. Li, R. Hendry, P. Samadi, and K. Bergman, “Scaling silicon photonic switch fabrics for data center interconnection networks,” *Optics Express*, vol. 23, p. 1159, Jan. 2015.

[14] L. Lu, L. Zhou, X. Li, and J. Chen, “Low-power 2x2 silicon electro-optic switches based on double-ring assisted Mach–Zehnder interferometers,” *Optics Letters*, vol. 39, p. 1633, Mar. 2014.

[15] P. Dong, C. Xie, L. L. Buhl, Y.-K. Chen, J. H. Sinsky, and G. Raybon, “Silicon In-Phase/Quadrature Modulator With On-Chip Optical Equalizer,” *Journal of Lightwave Technology*, vol. 33, pp. 1191–1196, Mar. 2015.

[16] C. Chen, C. He, D. Zhu, R. Guo, F. Zhang, and S. Pan, “Generation of a flat optical frequency comb based on a cascaded polarization modulator and phase modulator,” *Optics Letters*, vol. 38, p. 3137, Aug. 2013.

[17] Y. Urino, Y. Noguchi, M. Noguchi, M. Imai, M. Yamagishi, S. Saitou, N. Hirayama, M. Takahashi, H. Takahashi, E. Saito, T. Shimizu, M. Okano, N. Hatori, M. Ishizaka, T. Yamamoto, T. Baba, T. Akagawa, S. Akiyama, T. Usuki, D. Okamoto, M. Miura, J. Fujikata, D. Shimura, H. Okayama, H. Yaegashi, T. Tsuchizawa, K. Yamada, M. Mori, T. Horikawa, T. Nakamura, and Y. Arakawa, “Demonstration of 12.5-Gbps Optical Interconnects Integrated with Lasers, Optical Splitters, Optical Modulators and Photodetectors on a Single Silicon Substrate,” *Optics Letters*, p. Tu.4.E.1, 2012.

[18] C.-M. Chang, J. H. Sinsky, P. Dong, G. de Valicourt, and Y.-K. Chen, “High-power dual-fed traveling wave photodetector circuits in silicon photonics,” *Optics Express*, vol. 23, p. 22857, Aug. 2015.

[19] S. Garcia and I. Gasulla, “Design of heterogeneous multicore fibers as sampled true-time delay lines,” *Optics Letters*, vol. 40, p. 621, Feb. 2015.

[20] M. Mattarei, A. Canciamilla, S. Grillanda, and F. Morichetti, “Variable Symbol-Rate DPSK Receiver Based on Silicon Photonics Coupled-Resonator Delay Line,” *Journal of Lightwave Technology*, vol. 32, pp. 3317–3323, Oct. 2014.

[21] S. Janz, A. Densmore, D.-x. Xu, P. Waldron, J. Lapointe, G. Lopinski, T. Mischki, P. Cheben, A. Delâge, B. Lamontagne, and J. H. Schmid, “Silicon Waveguide Photonics for Biosensing Applications,” *Optics Letters*, p. IWA1, 2007.

[22] G. Lim, U. P. DeSilva, N. R. Quick, and A. Kar, “Laser optical gas sensor by photoexcitation effect on refractive index,” *Applied Optics*, vol. 49, p. 1563, Mar. 2010.

[23] E. Ryckeboer, R. Bockstaele, M. Vanslembrouck, and R. Baets, “Glucose sensing by waveguide-based absorption spectroscopy on a silicon chip,” *Biomedical Optics Express*, vol. 5, p. 1636, May 2014.

[24] B. Jalali and S. Fathpour, “Silicon Photonics,” *Journal of Lightwave Technology*, vol. 24, pp. 4600–4615, Dec. 2006.

[25] “Silicon photonics market to grow at CAGR of 38% from $25m in 2013 to $700m in 2024.” `http://www.semiconductor-today.com/news_items/2014/JUL/YOLE_180714.shtml`, 2014. [Online; accessed 06-Feb-2016].

[26] D. J. Richardson, J. M. Fini, and L. E. Nelson, “Space-division multiplexing in optical fibres,” *Nat Photon*, vol. 7, pp. 354–362, May 2013. Review.

[27] J. Hecht, “Is Keck’s Law Coming to an End?.” `http://spectrum.ieee.org/semiconductors/optoelectronics/is-kecks-law-coming-to-an-end`, Jan. 2016. [Online; accessed 18-Feb-2016].

[28] A. Xie, L. Zhou, J. Chen, and X. Li, “Efficient silicon polarization rotator based on mode-hybridization in a double-stair waveguide,” *Optics Express*, vol. 23, p. 3960, Feb. 2015.

[29] A. V. Velasco, M. L. Calvo, P. Cheben, A. Ortega-Moñux, J. H. Schmid, C. A. Ramos, i. M. Fernandez, J. Lapointe, M. Vachon, S. Janz, and D.-X. Xu, “Ultracompact polarization converter with a dual subwavelength trench built in a silicon-on-insulator waveguide,” *Optics Letters*, vol. 37, p. 365, Feb. 2012.

[30] D. Leung, B. Rahman, and K. Grattan, “Numerical Analysis of Asymmetric Silicon Nanowire Waveguide as Compact Polarization Rotator,” *IEEE Photonics Journal*, vol. 3, pp. 381–389, June 2011.

[31] J. Wang, B. Niu, Z. Sheng, A. Wu, X. Wang, S. Zou, M. Qi, and F. Gan, “Design of a SiO_2 top-cladding and compact polarization splitter-rotator based on a rib directional coupler,” *Optics Express*, vol. 22, p. 4137, Feb. 2014.

[32] D. Dai and J. E. Bowers, “Novel concept for ultracompact polarization splitter-rotator based on silicon nanowires,” *Optics Express*, vol. 19, p. 10940, May 2011.

[33] J. C. Wirth, J. Wang, B. Niu, Y. Xuan, L. Fan, L. Varghese, D. E. Leaird, and A. Weiner, “Efficient Silicon-on-Insulator Polarization Rotator based on Mode Evolution,” *Optics Letters*, p. JW4A.83, 2012.

[34] L. Chen, C. R. Doerr, and Y.-K. Chen, “Compact polarization rotator on silicon for polarization-diversified circuits,” *Optics Letters*, vol. 36, p. 469, Feb. 2011.

[35] J. D. Sarmiento-Merenguel, R. Halir, X. Le Roux, C. Alonso-Ramos, L. Vivien, P. Cheben, E. Durán-Valdeiglesias, I. Molina-Fernández, D. Marris-Morini, D.-X. Xu, J. H. Schmid, S. Janz, and A. Ortega-Moñux, “Demonstration of integrated polarization control with a 40 dB range in extinction ratio,” *Optica*, vol. 2, p. 1019, Dec. 2015.

[36] M. Ibrahim, J. H. Schmid, A. Aleali, P. Cheben, J. Lapointe, S. Janz, P. J. Bock, A. Densmore, B. Lamontagne, R. Ma, D.-X. Xu, and W. N. Ye, "Athermal silicon waveguides with bridged subwavelength gratings for TE and TM polarizations," *Optics Express*, vol. 20, p. 18356, July 2012.

[37] Q. Xu, L. Chen, M. G. Wood, P. Sun, and R. M. Reano, "Electrically tunable optical polarization rotation on a silicon chip using Berry's phase," *Nature Communications*, vol. 5, p. 5337, Nov. 2014.

[38] "Wave–particle duality." `https://en.wikipedia.org/wiki/Wave%E2%80%93particle_duality`, Jan. 2016. [Online; accessed 07-Feb-2016].

[39] "Maxwell's equations." `https://en.wikipedia.org/w/index.php?title=Maxwell%27s_equations&oldid=702587090`, Jan. 2016. [Online; accessed 07-Feb-2016].

[40] G. T. Reed, *Silicon Photonics: The State of the Art.* New York, NY, USA: Wiley-Interscience, 2008.

[41] J. M. Burch and A. Gerald, *Introduction to Matrix Methods in Optics.* John Wiley & Sons, 1st ed., 1975.

[42] F. Flossmann, U. T. Schwarz, M. Maier, and M. R. Dennis, "Stokes parameters in the unfolding of an optical vortex through a birefringent crystal," *Optics Express*, vol. 14, no. 23, p. 11402, 2006.

[43] "Optical polarization waves." `http://www.wikiwand.com/en/Polarization_(waves)`, 2015. [Online; accessed 09-Feb-2016].

[44] J. M. Kahn, K.-P. Ho, and M. B. Shemirani, "Mode coupling effects in multi-mode fibers," in *Optical Fiber Communication Conference*, p. OW3D.3, Optical Society of America, 2012.

[45] H. Haus and W. Huang, "Coupled-mode theory," *Proceedings of the IEEE*, vol. 79, pp. 1505–1518, Oct 1991.

[46] Y. Ding, H. Ou, and C. Peucheret, "Wideband polarization splitter and rotator with large fabrication tolerance and simple fabrication process," *Opt. Lett.*, vol. 38, pp. 1227–1229, Apr 2013.

[47] J. Zhang, M. Yu, G.-Q. Lo, and D.-L. Kwong, "Silicon-waveguide-based mode evolution polarization rotator," *Selected Topics in Quantum Electronics, IEEE Journal of*, vol. 16, pp. 53–60, Jan 2010.

[48] H. "Zhang, S. Das, J. Zhang, Y. Huang, C. Li, S. Chen, H. Zhou, M. Yu, P. Guo-Qiang Lo, and J. T. L. Thong, "Efficient and broadband polarization rotator using horizontal slot waveguide for silicon photonics," *Applied Physics Letters*, vol. 101, no. 2, 2012.

[49] J. C. Wirth, J. Wang, B. Niu, Y. Xuan, L. Fan, L. Varghese, D. E. Leaird, and A. Weiner, "Efficient silicon-on-insulator polarization rotator based on mode evolution," *Conference on Lasers and Electro-Optics 2012*, p. JW4A.83, 2012.

[50] K. Goi, A. Oka, H. Kusaka, K. Ogawa, T.-Y. Liow, X. Tu, G.-Q. Lo, and D.-L. Kwong, "Low-loss partial rib polarization rotator consisting only of silicon core and silica cladding," *Opt. Lett.*, vol. 40, pp. 1410–1413, Apr 2015.

[51] H. Fukuda, K. Yamada, T. Tsuchizawa, T. Watanabe, H. Shinojima, and S. ichi Itabashi, "Polarization rotator based on silicon wire waveguides," *Opt. Express*, vol. 16, pp. 2628–2635, Feb 2008.

[52] D. Vermeulen, S. Selvaraja, P. Verheyen, P. Absil, W. Bogaerts, D. Van Thourhout, and G. Roelkens, "Silicon-on-insulator polarization rotator based on a symmetry breaking silicon overlay," *Photonics Technology Letters, IEEE*, vol. 24, pp. 482–484, March 2012.

[53] Z. Wang and D. Dai, "Ultrasmall Si-nanowire-based polarization rotator," *Journal of the Optical Society of America B*, vol. 25, p. 747, May 2008.

[54] M. Aamer, A. Gutierrez, A. Brimont, D. Vermeulen, G. Roelkens, J.-M. Fedeli, A. Hakansson, and P. Sanchis, "CMOS Compatible Silicon-on-Insulator Polarization Rotator Based on Symmetry Breaking of the Waveguide Cross Section," *IEEE Photonics Technology Letters*, vol. 24, pp. 2031–2034, Nov. 2012.

[55] R. Y. Chiao and Y.-S. Wu, "Manifestations of berry's topological phase for the photon," *Phys. Rev. Lett.*, vol. 57, pp. 933–936, Aug 1986.

[56] A. Tomita and R. Y. Chiao, "Observation of berry's topological phase by use of an optical fiber," *Phys. Rev. Lett.*, vol. 57, pp. 937–940, Aug 1986.

[57] CST Development Core Team, *CST: 3D EM simulation software.* Computer Simulation Technology, Darmstadt, Germany, 2016.

[58] C. Errando-Herranz, F. Niklaus, G. Stemme, and K. Gylfason, "A low-power MEMS tunable photonic ring resonator for reconfigurable optical networks," in *2015 28th IEEE International Conference on Micro Electro Mechanical Systems (MEMS)*, pp. 53–56, Jan. 2015.